Materials & Design 264 (2026) 115756

Contents lists available at ScienceDirect

Materials & Design

journal homepage: www.elsevier.com/locate/matdes

Effect of microstructural heterogeneity on the strengthening and fracture mechanism in in-situ cast TiC/Al composites

Wojciech Maziarz [a,*], Robert Chulist [b], Ganna Chyzhyk [a,f], Anna Wojcik [b], Pawel Kurtyka [c], Sebastian Sobula [e], Norbert Schell [d], Ewa Olejnik [c,e]

[a] Institute of Metallurgy and Materials Science of the Polish Academy of Sciences, Reymonta 25 Str. 30-059 Krakow, Poland
[b] Faculty of Metals Engineering and Industrial Computer Science, AGH University of Krakow, al. A. Mickiewicza 30, 30-059 Krakow, Poland
[c] Innerco Sp. z o.o., Siwka 17 Str. 31-588 Krakow, Poland
[d] Institute of Materials Physics, Helmholtz-Zentrum Hereon, Max-Planck-Strasse 1, D-21502 Geesthacht, Germany
[e] Faculty of Foundry Engineering, AGH University of Krakow, al. A. Mickiewicza 30, 30-059 Krakow, Poland
[f] G.S. Pysarenko Institute for Problems of Strength of the National Academy of Sciences of Ukraine, Sadowo-Botanichna 2 Str., 01014 Kyiv, Ukraine

ARTICLE INFO

Keywords:
Metal Matrix Composities
Casting
Strengthening mechanism
Wear
TEM
X-Ray diffraction

ABSTRACT

Structural heterogeneity is an inherent feature that occurs practically in all cast materials. In this work, we demonstrated that the chemical heterogeneity resulting from the SHS reaction of TiC formation in the aluminum Al1000 alloy bath can enhance the strength by refining the matrix grains in *in-situ* cast TiC/Al1000 composites. Using advanced characterization techniques including X-Ray synchrotron radiation diffraction, (S)TEM-HREM and SEM-EBSD studies, we identified two types of aluminum solid solutions within the dendritic grains of the Al1000 matrix, distinguished by different lattice parameters. These differences result from the presence of unreacted titanium, which locally forms a supersaturated solid solution in the form of nanoprecipitates with a size of about 10 nm and a smaller lattice parameter compared to titanium-free regions. Another structural heterogeneity influencing the mechanical properties and fracture of composites is the agglomeration of TiC particles driven by the pushing and engulfment of particles at the crystallization front. Fractographic analysis revealed a correlation between mechanical properties and wear resistance in TiC/Al1000 composites with TiC contents ranging from 5 to 15 vol%. In samples with more than 10 vol% TiC, particle agglomeration contributed to increased strength but reduced ductility, due to weakened interfacial bonding and non-uniform deformation under load.

1. Introduction

Fabrication of metal matrix composites (MMCs) by *in-situ* casting techniques has attracted much attention since it offers significant advantages over *ex-situ* methods including fine particle size, clean interface, and good wettability of the reinforcement with the matrix as well as homogeneous distribution of the reinforcement. However, the most important aspect is the ability to control microstructural elements by adjusting the processing conditions. Among the several groups of composite materials produced via *in-situ* methods, aluminum metal matrix composites (Al-MMCs) are one of the most widely studied, encompassing numerous matrix compositions and types of reinforcing particles [1–6]. They found many importants applications in the automotive and aerospace industries as well as in electrical engineering due to their unique combination of properties e.g. high strength-to-weight ratio, elastic modulus, low thermal coefficient, excellent corrosion resistance, and wear resistance. It is well known that the microstructure of the composites, determining their strength and ductility, is primarily controlled by processing conditions during fabrication [7]. In one of the most effective process – the Self-propagating High-temperature Synthesis (SHS) – a key factor influencing the final microstructure is the interaction between the solidification front and the particles [8]. This phenomenon is called particle pushing and engulfment phenomenon or interaction between a solid particle and advancing solid/liquid interface. This interaction largely determines the uniformity of nanoparticle distribution in the composite [9,10]. The nonuniform distribution of the nanoparticles in MMCs is commonly explained by particle pushing by the advancing solid, liquid interface during solidification. As the melt

* Corresponding author.
E-mail address: w.maziarz@imim.pl (W. Maziarz).

https://doi.org/10.1016/j.matdes.2026.115756
Received 20 October 2025; Received in revised form 22 December 2025; Accepted 27 February 2026
Available online 28 February 2026

solidifies, particles may be pushed ahead of the interface, engulfed by the solid, or trapped between dendrite arms [11]. This often leads to particle agglomeration at grain boundaries, while grain interiors remain nearly particle-free, resulting in limited reinforcement after solidification [12,13]. As a consequence, practically no reinforcement after solidification is achieved. Therefore, the effective nanoparticle dispersion involves two key steps: achieving a uniform particle distribution in the liquid metal and retaining the particles during solidification. On the other side, the uniform dispersion in the melt requires overcoming van der Waals forces and reducing particle agglomeration, which is commonly achieved by ultrasonic treatment or electromagnetic stirring during induction melting [14]. Dispersion stability also depends on sufficient interfacial energy and good wettability between the melt and the nanoparticles. During the solidification, nanoparticles can be captured either by increasing melt viscosity to reduce particle pushing [15] or by using nanoparticles with a higher Hamaker constant than the liquid metal, such as core–shell particles, which promotes their spontaneous engulfment by the solid phase [16]. In our previous work [17] we demonstrated that a modified SHSB process can be used to cast aluminium-based composites reinforced with TiC and (Ti,W)C nanoparticles. The process is controlled by adding a moderator that influences supercooling, thereby affecting the nucleation and growth of TiC particles. By adjusting the moderator amount, the size, quantity, and distribution of reinforcing particles can be tailored. Till now, many reports have been focused on the tailoring the amount, size and distribution of the in-situ synthesized ceramic phases, including SiC [18,19], Al_2O_3 [20,21], TiC [22] as well as B_4C [23,24] in metals matrices and their impact on mechanical properties. For many years, the primary goal of research was to produce materials with a uniform distribution of reinforcement within the metal matrix to achieve high strength while high ductility seemed to be achieved by a fine size of the reinforcing particles. However, even when the reinforcing particles were very fine and homogeneously embedded in the matrix, a loss of ductility was often observed. To overcome this limitation, a new strategy has been proposed, in which a favorable combination of strength and ductility is achieved by controlling particle distribution and designing a tailored microstructural architecture. Typical architectures reported in the literature include so-called heterostructures, such as tri-modal structures, “composite within a composite” designs, and layered structures [25–30]. In these materials, an inhomogeneous microstructure is intentionally created, with “soft” regions responsible for ductility and “hard” regions providing high strength.

Finally, it is well known that several strengthening mechanisms contribute to the improved mechanical properties of MMCs: (i) load-bearing strengthening, (ii) Orowan strengthening, (iii) Hall-Petch strengthening, and (iv) dislocation density difference induced by the Coefficient of Thermal Expansion (CTE) mismatch during fabrication. The load-bearing strengthening occurs when the applied external load is transferred from the soft matrix to the stiff and hard nanoparticles, contributing to the overall strengthening of the nanocomposites [31]. Orowan strengthening is another significant mechanism for reinforcing MMCs [32] in which closely spaced hard nanoparticles impede dislocation motion. These non–shearable ceramic particles pin crossing dislocations, forcing them to bow around the particles under external loading, which increases the composite’s strength. Hall-Petch strengthening results from grain refinement. Dislocations moving from one grain to another with different crystallographic orientations must change the direction and slip system [33], which increases resistance to deformation and contributes to strength improvement [34,35]. The last mechanism, generally considered less significant for strengthening of Metal Matrix Nano Composites (MMNCs), especially when nanoscale reinforcements are used, is CTE mismatch [36]. All above mentioned strengthening mechanisms play a role in reinforcing the matrix of the composite, but with different degrees of effectiveness. The most effective strengthening mechanisms in MMNCs are Orowan and Hall–Petch, while load-bearing and CTE mismatch contribute to a lesser extent. The increase in strength may result from a combination of the aforementioned strengthening mechanisms, with the Orowan mechanism appearing to be the most effective [37]. In this study, the additional strengthening effect associated with chemical heterogeneity of Ti dissolved in the Al matrix, observed in *in-situ* MMCs, is deeply investigated. This effect related to supersaturation of Ti may be interpreted as a combination of Hall-Pech (grain size reduction in saturated regions), Orowan (enhanced lattice misfit and increased dislocation generation) and solution strengthening mechanisms (higer Ti contration), opening new perspectives in the design of *in-situ* cast composites. We propose that, this phenomenon mainly occurs in the case of *in-situ* casting, due to the highly exothermic and non-equilibrium nature of TiC formation, in which not all of the titanium is consumed during the reaction. Nevertheless, similar effects may also arise in other particle–matrix systems produced via SHS, rendering this mechanism universal and relevant for the further development of MMCs. The influence of TiC volume fraction on mechanical properties, hardness and wear resistance is also studied. Finally, fracture surface examination at critical TiC content enables to explain the dominant fracture mechanisms and the observed variations in strength and ductility.

2. Experimental procedure

The composites based on the aluminum Al1000 alloy were produced using Ti and C powders as reactants, with initial weight percentages added to achieve nominal TiC volume fractions of 5%, 10%, and 15% according to the detailed procedure presented in [17]. The *in-situ* reactions for synthesizing the TiC particulates reinforcement in the Al-Ti-C system was proposed by Nukami and Flemings [38] based on DTA and XRD analysis. Similarly to our case the particulate TiC-reinforced aluminum composite specimens were processed by compacting a mixture of titanium, carbon, and additionally aluminum powders into preforms that were infiltrated with molten aluminum. During heating of an aluminum infiltrated preform, an exothermic reaction $Ti + 3Al = TiAl_3$ occurs between about 890 and 990 K. Synthesis of TiC particles by the reaction $3TiAl_3 + Al_4C_3 = 3TiC + 13Al$ occurs at about 1150 K and by the reaction $TiAl_3 + C = TiC + 3Al$ occurs continuously up to about 1265 K. The The structure, phase composition were examined by high-energy X-ray diffraction measurements at DESY in Germany, Hamburg, using the beamline P07B (87.1 keV, $\lambda = 0.0142342$ nm). The casting concept is shown in Fig. 1 along with a sample cutting schema indicating the locations from which the samples were spark-eroded for different analyses. The lattice parameters of the matrix and volume fraction TiC were calculated by Rietveld analysis and High Score Plus software [39,40]. Microstructural observations were carried out by FEI Quanta 3D field emission gun scanning electron microscope (SEM) equipped with Trident energy dispersive X-ray spectrometer (EDX) produced by EDAX and TSL electron backscattered diffraction (EBSD). The fracture surface of samples after tensile tests was investigated by SEM FEI E-SEM XL30. The detailed microstructural characterization, including determination of the crystal structure and high-resolution observations at the atomic scale, was performed by use of transmission electron microscopes (TEM) FEI Tecnai G2 200 kV and Thermo Fisher Titan Themis 200 G3. Samples for SEM observations were mechanically and then electrolytically polished at room temperature with a Struers electropolishing LectroPol-5 using an electrolyte of nitric acid (vol. 1/3) and methanol (vol. 2/3). Samples for TEM in the form of lamellas were prepared by Focused Ion Beam (FIB) method using Thermo Fisher Scios 2 Focus Ion Beam Scanning Electron Microscope. The mechanical properties of the composites were determined in the tensile tests using an Instron TT-DM machine equipped with an electronic measuring system.

Tests were conducted at 293 K with an initial strain rate of $10^{-3}s^{-1}$. The hardness was measured using United Test hardness tester by applying the Vickers method using a load of 9.8 N (HV1) for 10 s. The abrasive wear resistance of the composite materials was assessed using

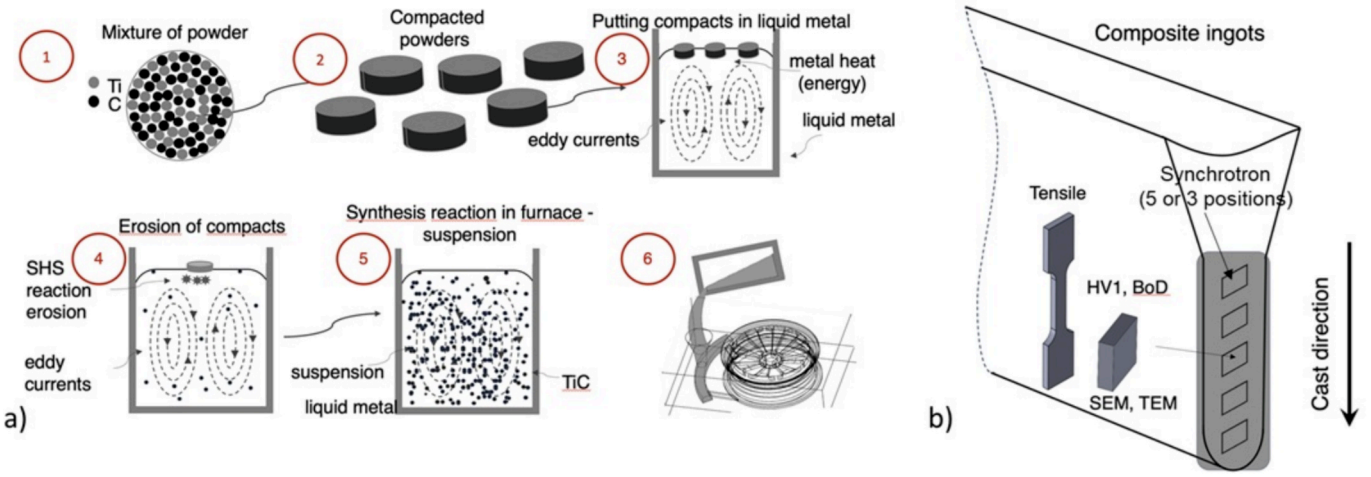

Fig. 1. (a) Casting concept showing the individual steps of the in situ process. (b) Sample cutting scheme indicating the locations from which the samples were spark-eroded.

the ball-on-disc method on an ELB-07 tribotester (ELBIT, Poland) based on ISO 20808:2004(E) standards. The main test parameters were as follows: Al_2O_3 ball with a diameter of 3 mm, friction track diameter of approximately 3.5 mm, disc rotational speed of 192 rpm and loading force of 4 N. Each test was conducted at room temperature for 10,000 s. The wear volume was measured by Keyence VHX 7000 digital microscope.

3. Results and discussion

The strengthening mechanism in aluminum-based composites is attributed to several factors: (i) the volume fraction and particle size of TiC (contributing to load-bearing and Orowan strengthening), (ii) grain refinement of the matrix (via Hall–Petch strengthening) and (iii) the lattice mismatch between the aluminum matrix and TiC particles. In our recent study [41], we analyzed all of the aforementioned mechanisms based on the multiscale microstructural investigations of two Al-based composites containing 5 and 15% TiC particles. The results are consistent with commonly accepted strengthening principles for metal matrix composites [42]. However, further detailed microstructural and structural studies revealed new previously unreported phenomena that may influence the mechanical properties of the investigated composites. Fig. 2 (a-c) shows the set of SEM BSE micrographs acquired at different magnifications for the composite fabricated with a nominal 5 vol% TiC content.

The microstructure is typical of metal matrix composites, with reinforcement particles predominantly located in the interdendritic regions, and a smaller fraction embedded within the dendritic grains. In addition, contrast variations are visible within the dendritic grains, likely resulting from variation in chemical composition and grain orientation. At the higher magnification, distinct differences in grain size across various regions are clearly observable. Moreover, the line scan shown in Fig. 2d indicates an increased Ti content in the brighter regions, demonstrating that the flower-type regions are enriched in Ti. The phase map image shown in Fig. 3a confirmed that the TiC particles are mainly distributed in the inter-dendritic spaces, however, some of them also occur inside the dendrite grains. The total volume fraction of TiC particles, determined by X-ray analysis, is 4.2 vol%, which is slightly lower than the nominal value due to the density difference between the introduced TiC reactants and the final TiC particles. The same area fraction was calculated from image analysis which remains below 5%, as shown in Fig. 4. This indicates that not all of the titanium and graphite were consumed during the SHS reaction, and the reaction yield was therefore less than 100%. Similar trends are observed for composites containing 10 and 15 vol% TiC, as shown in Fig. 4. SEM EBSD examination performed in the area shown in Fig. 3b confirmed that the contrast visible in Fig. 2c is due to grain orientation. The dendritic grains, which feature submicron grains, are characterized by random orientations and both low- and high-angle grain boundaries (Fig. 3 (a-c)). The misorientation profile shown in Fig. 3c indicates significant misorientation reaching up to 60° and notable grain refinement with a mean grain size below 1 μm.

In order to determine the crystal structure of both the matrix and TiC particles, as well as to calculate the volume fraction and lattice parameters of each phase, the high-energy synchrotron radiation diffraction and subsequent Rietveld analysis were performed. Fig. 5 presents a set of high-energy X-ray diffraction patterns for the Al-based composite acquired at five different points, together with the analysis of (222) Al

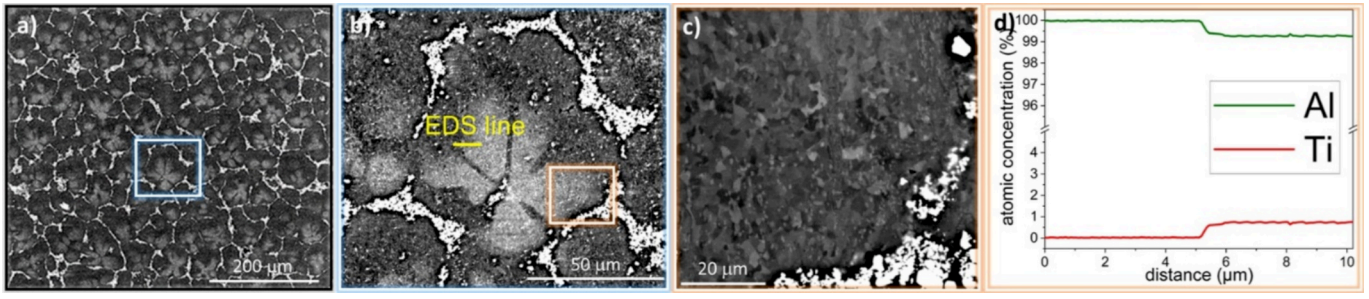

Fig. 2. (a–c) SEM images acquired in backscattered electron (BSE) mode of composite with a nominal 5 vol% of TiC at different magnifications, revealing characteristic compositional contrast variations within the dendritic grains; (d) EDS line scan performed along the yellow line marked in Fig. 1b. (For interpretation of the references to colour in this figure legend, the reader is referred to the web version of this article).

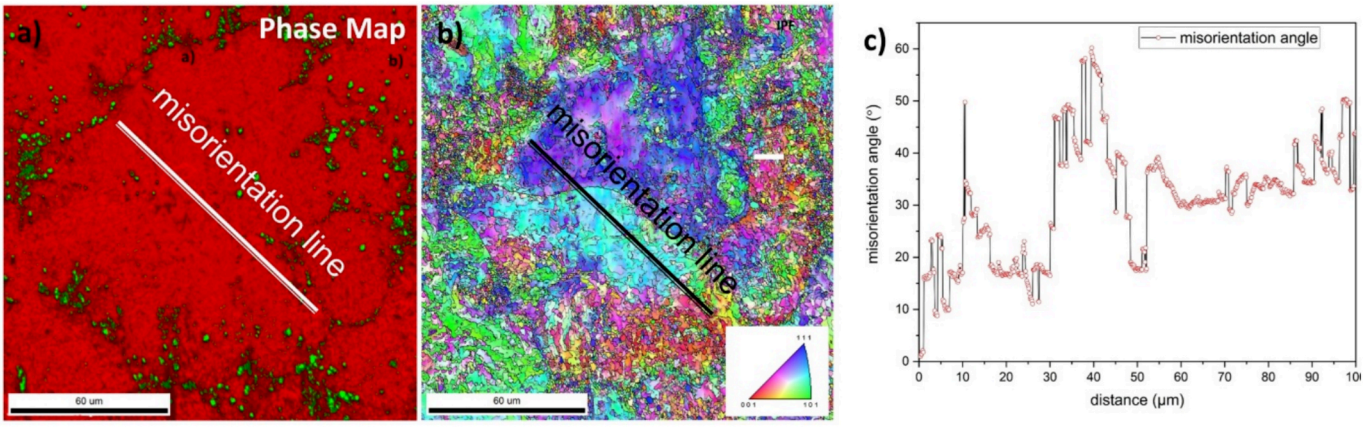

Fig. 3. (a) EBSD phase map; (b) inverse pole figure (IPF) orientation map with the corresponding misorientation profile; (c) distribution of the misorientation angle measured along the line indicated in (b).

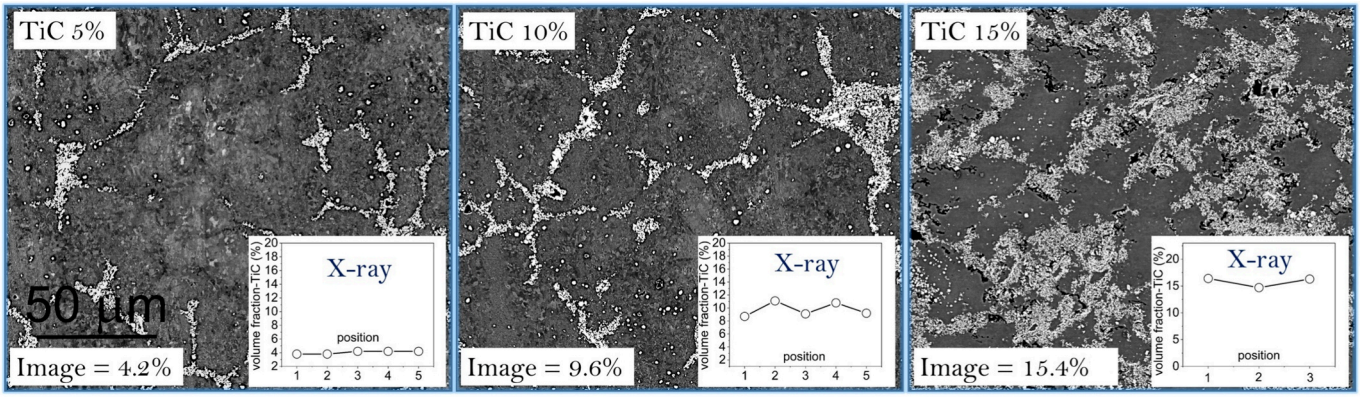

Fig. 4. Series of SEM-BSE images for samples with nominal TiC contents of 5%, 10%, and 15%, together with the corresponding TiC volume fractions calculated based on X-ray diffraction data and image analysis.

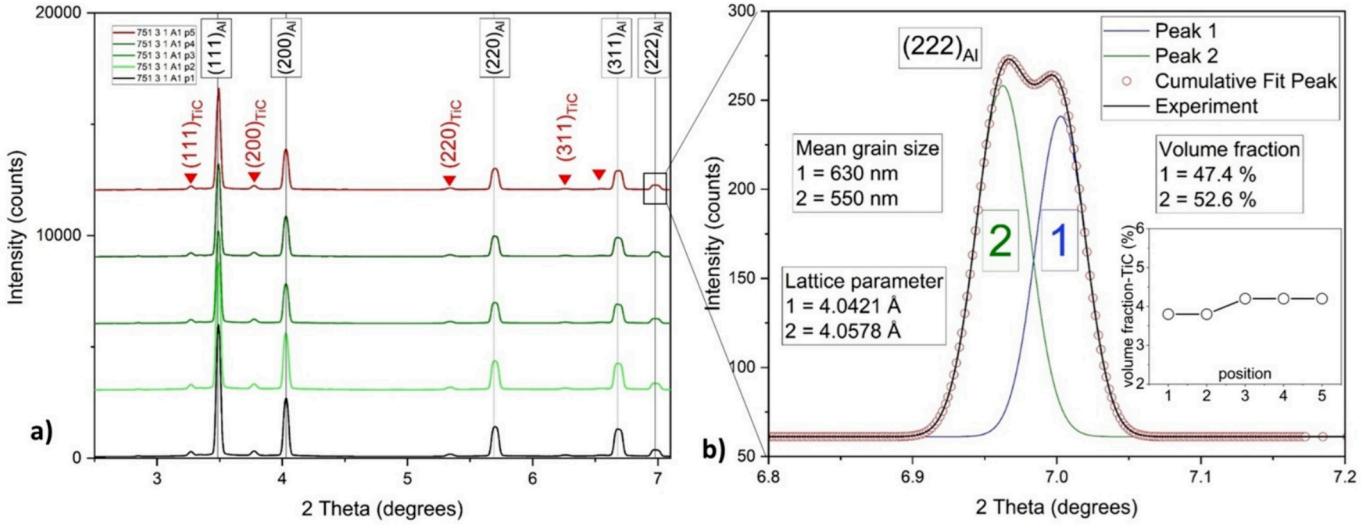

Fig. 5. Set of X-Ray synchrotron radiation diffraction patterns recorded at five different positions of sample (a), result of Rietveld analysis of (222) Al matrix peak (b) and plot showing volume fraction of TiC phase calculated for individual measuring positions (c).

matrix peak.

The diffractograms appear almost identical, for each point, indicating good homogeneity of the composite. The volume fraction of TiC particles varies slightly between 3.8 and 4.2% at all five points, being consistent with the measurements obtained from SEM BSE observations (4.2%) (Fig. 4).

Interestingly, the broadening of the peaks corresponding to (220), (311) and (222) planes of Al matrix is visible. This is clearly visible in

Fig. 5b, where the (222) peak was subjected to the Rietveld refinement procedure and then deconvoluted into two peaks with maxima located at different values of 2Theta. These positions can be attributed to two lattice parameters of the Al matrix $a_1 = 4.0421$ Å and $a_2 = 4.0578$ Å, with volume fractions of 47.4% and 52.6%, respectively.

Additionally, the deconvoluted peaks show differences in shape due to varying full-width at half maximum (FWHM), which is particularly evident in their width. This reflects differences in grain size across regions with different lattice parameters. Based on this, the average grain size was calculated as $D_1 = 630$ nm for the peak/region 1, and $D_2 = 550$ nm for peak/region 2. In order to confirm synchrotron radiation diffraction studies, advanced microstructural analysis was conducted, mainly based on TEM. Since the observation area is important here, the thin foil for TEM observations was prepared by FIB method. This enabled precise selection of the observation area and ensured uniform sample thickness (approximately 80 nm), providing consistent conditions for EDS chemical analysis and high-resolution microstructure observations. Fig. 6(a) shows the location where the thin foil was cut, including both areas.

The elemental distribution maps reveal a uniform distribution of Al, C and O, whereas Ti exhibits segregation. A variation in Ti concentration is observed at the boundary between a single Al grain and the elongated ones, with Ti reaching up to 0.6 at.% in the single grain. According to the Ti-Al phase diagram [43], the maximum solubility of Ti in Al, significantly decreases from 0.7 at.% at 650°C [44] to a negligible level at room temperature which is consistent with the SEM/EDS analysis shown in Fig. 1d. Therefore, it can be assumed that the region of the single aluminum grain constitutes a supersaturated solid solution of titanium in aluminum. Furthermore, these types of grains are expected to exhibit higher strength compared to Ti-free grains due to solid solution strengthening. To confirm the formation of a supersaturated solid solution in the selected matrix grains, TEM observation including bright field (BF), selected area electron diffraction (SAED) and high resolution transmission electron microscopy (HR-TEM) were performed. Fig. 4 shows BF microstructures and corresponding SAED patterns taken from two areas (A1 and A2), both well indexed in accordance with the Al [013] zone axis. As the lamella was prepared across the area exhibiting different contrast, a clear difference is also evident in BF microstructure (Fig. 7a). A distinct boundary (marked with a dashed line) can be seen between elongated grains which are approximately 2 μm in length and 500 nm in width from the area with grains that are difficult to identify.

This area is most likely a single Al grain oriented along [103], similarly to the purple region shown in Fig. 3 (c). Fig. 7 (b) and (d) present BF microstructures taken at higher magnifications from regions R1 and R2, respectively. Although the BF microstructures were acquired under Bragg conditions, contrast variations associated with a high density of dislocations and/or precipitates are still visible. The significant differences are also visible in SAED patterns. As mentioned before, both regions have the same [103] Al zone axis, but in the case of region R2, additional diffusion streaks (marked by arrows) located between the main diffraction spots can be distinguished (Fig. 7 (e)). The presence of these streaks in the diffraction image suggests the presence of fine precipitates in the examined microstructure.

To confirm the presence (or absence) of precipitates in the analyzed regions, high-resolution HR-TEM studies were carried out. The HR-TEM images from the region R1 are presented in Fig. 8. The Reduced Fast Fourier Transform (FFT) image shows only diffraction spots corresponding to the (200) and (311) planes of Al with [013] zone axis. However, large contrast differences can be seen in the HR-TEM image, related to a high density of structural faults, including dislocations. This is clearly visible in the IFFT (Inverse Fast Fourier Transform) image taken from the selected area (indicated by white square in HR-TEM image) after noise reduction by applying the FFT image masking process. It can be seen that in the selected area there is a high density of dislocations (examples indicated by white circles) resulting from stresses/strains accompanying the movement of the crystallization front and the presence of previously formed TiC particles.

The results of HR-TEM analysis conducted in region R2 are presented in Fig. 9. In this case, the reduced FFT image generated from the entire HR-TEM micrograph reveals distinct additional reflections, indicated by arrows. Interestingly, this type of diffraction occurs only in specific regions. As shown, the diffraction patterns obtained from the yellow regions do not exhibit additional reflections, in contrast to the regions where these reflections are visible.

The additional reflections are connected with the occurrence of a supersaturated solid solution of titanium in aluminum, as shown in Fig. 9 (d), simulating the positions of the atom columns of Ti and Al in the magnified IFFT image, based on the diffraction vectors *g* and interplanar spacing measured from FFT image. Since additional reflections do not appear in all areas of the high-resolution images, it can be assumed that this supersaturated solid solution has a tendency to form precipitates approximately 10 nm in size (Fig. 9 (a) red square). This, in

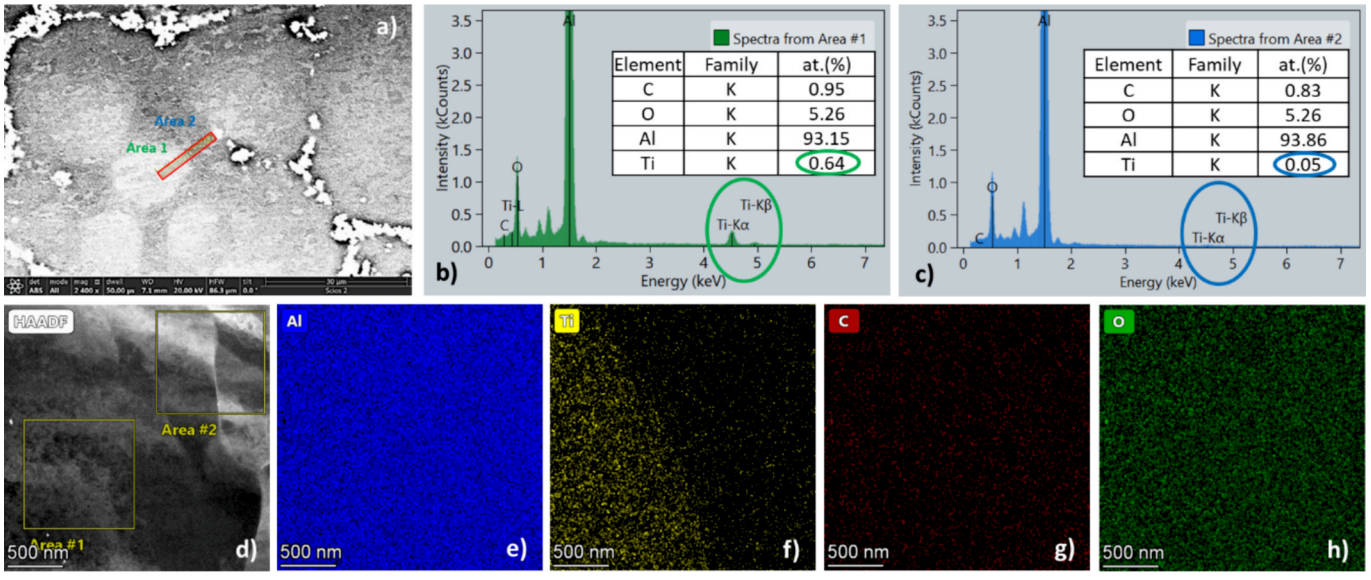

Fig. 6. (a) SEM BSE image with marked location of lamella cutting, (b) and (c) chemical composition results of taken from both Area 1 and Area 2, (d) STEM-HAADF image with marked both areas and (e-h) elemental mapping.

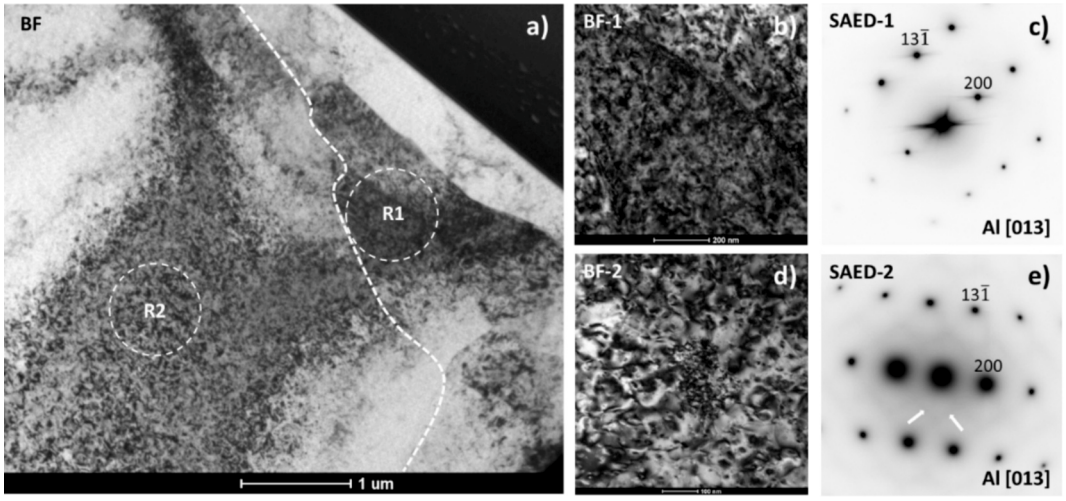

Fig. 7. (a) Lower magnification BF image and BF microstructures from regions R1 and R2 acquired with higher magnification (b), (d) and corresponding SEAD patterns (c), (e), respectively.

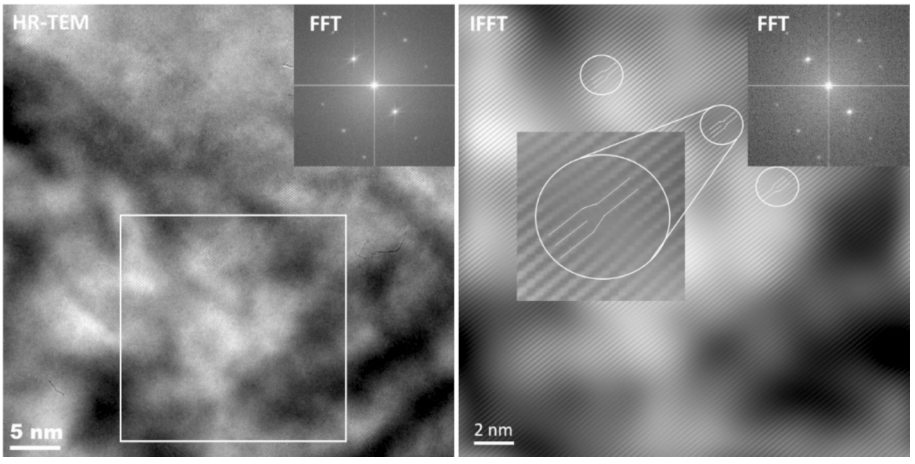

Fig. 8. HR-TEM, FFT and IFFT images taken from the region R1.

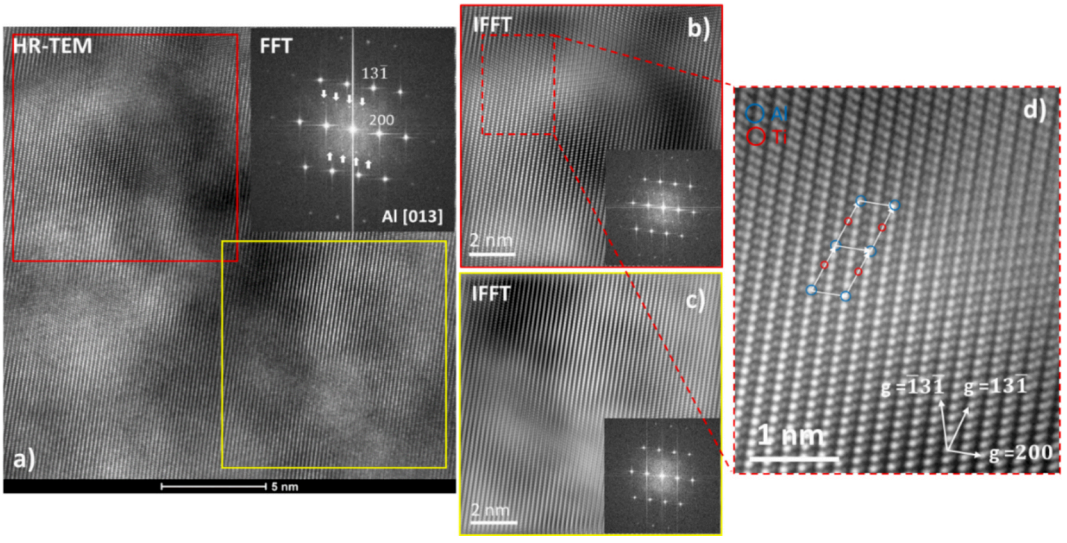

Fig. 9. (a) HR-TEM image and (b) corresponding reduced FFT, IFFT image generated from the red area in HR-TEM image, (c) IFFT image obtained from yellow area in HR-TEM image and (d) magnified area marked by red rectangle of IFF image. (For interpretation of the references to colour in this figure legend, the reader is referred to the web version of this article.)

consequence, causes the refinement of the matrix microstructure and strengthening of the entire composite. The presence of Ti atoms in the solid solution causes a change in the interplanar spacing of selected crystallographic planes, as shown in Fig. 10. It is visible that the additional reflections occurring between the (113) type planes of the Al solid solution result in a significant increase in the interplanar spacing d_{113} from 1.222 to 1.245 Å. This is not observed for (200) type planes, where there are no additional reflections, and the spacing remains similar, differing only in the magnitude due to measurement error.

Based on the above considerations and taking into account the pushing-engulfment phenomenon of TiC particles at the crystallization front during the in-situ fabrication of composites, a formation mechanism for the flower-type microstructure, as shown in Fig. 11, can be proposed. In the initial stage of in-situ casting, TiC particles are formed as a result of an exothermic reaction initiated in pure graphite and titanium powders, which are introduced into the molten aluminum in the form of compacts. A certain amount of unreacted Ti dissolves in liquid Al (in accordance to the Ti-Al phase diagram) due to the temperature increase caused by exothermic reaction. During cooling, the Al matrix begins to crystallize (forming the central part of the flower-type grain shown in Fig. 11), while the advancing crystallization front simultaneously pushes TiC particles outward, creating the surrounding region of the flower-type structure. Further cooling suppresses the diffusion of Ti atoms in the Al matrix due to the negligible solubility of Ti in Al at lower temperatures. The Al matrix supersaturated with Ti exhibits a larger lattice parameter than that of pure aluminum. As seen in Fig. 11, a single dendritic grain is surrounded by TiC particles located within the interdendritic regions. Due to the different lattice parameters of both the solid solutions and the TiC particles, a high level of internal stresses can be expected in the region of these solid solutions, inhibiting grain growth. As previously discussed, the newly found grain formation mechanism in TiC/Al1000 composites introduces two additional strengthening effects related to the grain refinement of the Al matrix and solution strengthening, which have not been incorporated into traditional models of composite strengthening to date.

In order to demonstrate the influence of strengthening mechanisms on hardness, strength, plasticity and resistance to abrasive wear, composites with a volume fraction of TiC particles ranging from 5 to 15 vol% were produced. The tensile strength curves, results of hardness and abrasion wear resistance measurements of these composites compared to of the cast aluminum of the Al1000 series are shown in Fig. 12. The stress–strain curves show that there are two types of samples, the first

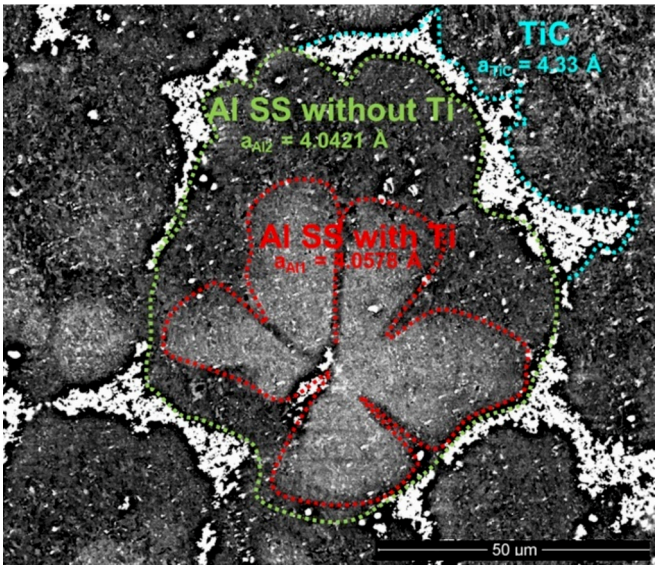

Fig. 11. SEM-BSE image of the flower-type microstructure with the marked ranges of occurrence of individual solid solutions and TiC particles.

with TiC particle content up to 10%, in which the strength improves by about 18% compared to the aluminum Al1000 alloy and relatively slight reduce in plasticity, and the second, containing 15 vol% TiC, in which there is a clear loss of plasticity with a simultaneous increase in strength, Fig. 12a. Additionally, there is an almost linear change in hardness and wear index (Fig. 12c). Such a division of the properties of the investigated composites suggests that they can be used as structural materials with improved strength and plasticity (TiC from 5 to 10 vol%) or functional materials with increased hardness and resistance to abrasive wear (15 vol% TiC). Changes in these properties are closely related to the microstructure of the analyzed composites. It was observed that the addition of more than 10 vol% TiC causes strong agglomeration of particles [27].

The different fracture mechanisms of composite samples containing 5 and 15 vol% of TiC particles as well as the initial aluminum alloy were analyzed by SEM observation of fracture surfaces after tensile tests, as presented in Fig. 13. The fracture surface of the initial Al alloy is characterized by a ductile, fibrous fracture with pronounced signs of plastic

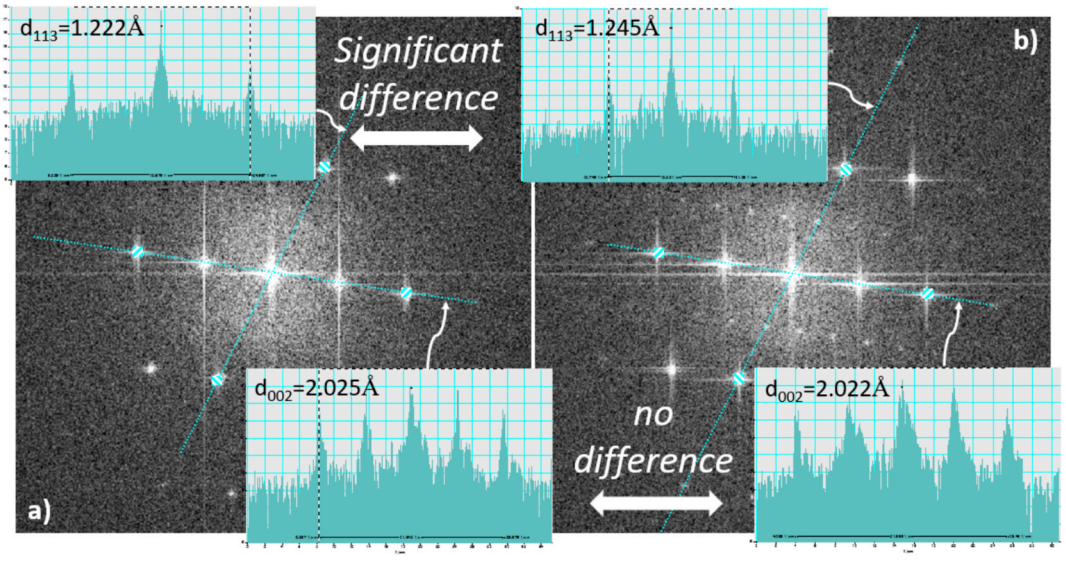

Fig. 10. FFT images for regions without (a) and with (b) the titanium in Al solid solution and results of measurement of interplanar spacings by the profile intensities along indicated lines.

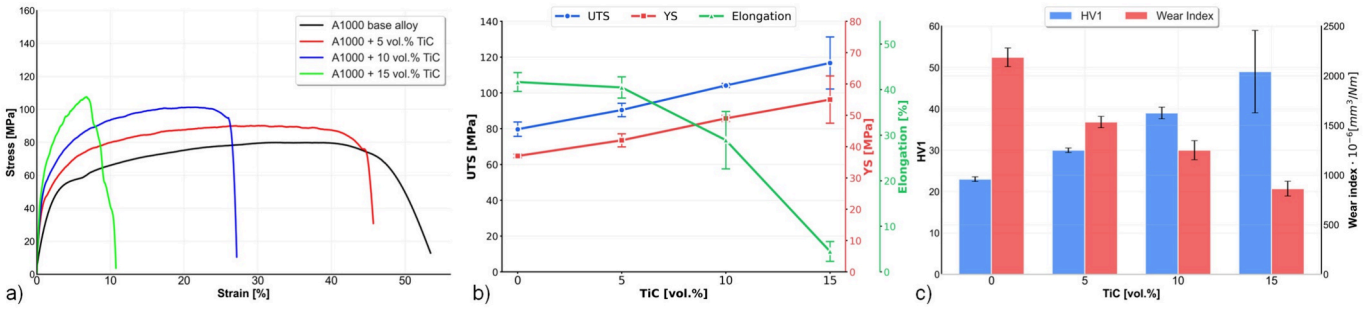

Fig. 12. Set of mechanical properties of aluminum Al1000 series alloy and composites containing 5–15 vol% TiC, tensile strain–stress curves a) results of micro hardness measures, UTS-ultimate tensile strength, YS-yeald stress and A-starin b), along with HV and wear index c).

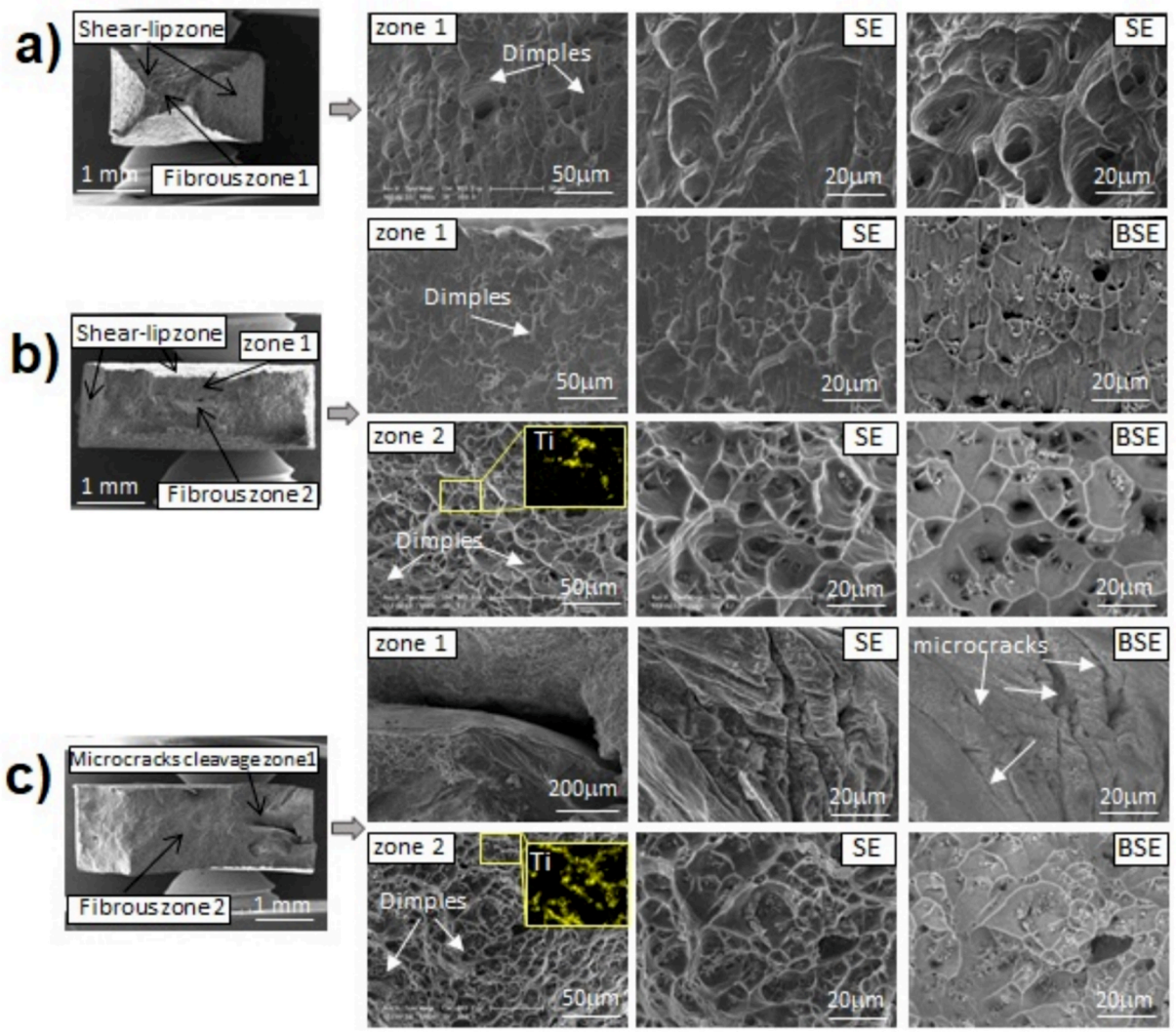

Fig. 13. Fracture surface of samples after tensile tests for a) the initial aluminum alloy, b) composite containing 5 vol% of TiC particles c) composite containing 15 vol% of TiC particles.

deformation (Fig. 13 (a)). The shear-lip zone occupies about two-thirds of the total fracture area. The central fibrous region is composed of deep dimples with diameters varying between 7 to 45 µm. Some individual dimples reach depths of 55–60 µm along the direction of the applied load, indicating high ductility and relatively low strength. For the specimen containing 5 vol% of TiC, tensile loading results in a typical cup-and-cone fracture. The presence of a second phase (inclusions) alters the fracture morphology compared to the pure metal. The fracture surface lies almost entirely in a plane normal to the sample axis. In this region (Zone 2 in Fig. 13 (b)), a dimpled relief is observed. The fracture surface of the specimen with 5 vol% TiC formed as a result of cavity initiation in the matrix during testing (dimples up to 30 µm in size), along with the formation of small pores (1–3 µm) at the TiC particle sites, which subsequently coalesced.

The shape of the dimples on the fracture surfaces of the tensile-tested samples is characteristic, indicating the dominance of maximum

principal stresses. In the peripheral areas of the fracture surface (zone 1), inclined at an angle, the resulting dimples are more elongated in the applied load direction and formed due to maximum shear stresses. The location of TiC inclusions is also clearly visible in the BSE images. In general, at the micro level, the fracture surface is homogeneous, and the fracture is ductile. The dimples are smaller and shallower compared to the initial sample. No brittle fracture areas or cracks were observed on the fracture surface, which indicates effective interaction between the inclusions and the matrix, as well as their uniform and finely dispersed distribution. This is most likely due to both the size and spatial distribution of the inclusions, which do not cause significant local stress concentrations. This observation aligns with the findings of the other researchers [45,46], who reported that coarse inclusions lead to higher stress concentrations during loading, promoting crack initiation and reducing ductility. In contrast, finely dispersed inclusions increase the probability of smaller dimples forming, thereby contributing to the improvement of the alloy's mechanical properties [47]. Therefore, the addition of 5 vol% TiC allows the studied alloy to retain sufficient ductility while achieving higher strength compared to the aluminum Al1000 series. The fracture surface of the composite containing 15 vol% TiC is characterized by noticeable heterogeneity in both macro- and microrelief. In addition to the ductile fracture zone with a dimpled microrelief, there is also significant microstructural splitting (approximately 800 μm in length) and secondary cracks located in areas of stress concentration (Zone 1 in Fig. 13 (c)). As was mentioned before, increasing the TiC content to 15 vol% leads to the formation of agglomerates [32]. J. Yang et al. observed the negative effects of precipitate agglomeration on the mechanical properties of composites [48]. Although a greater amount of TiC inclusions acts as barriers to dislocation movement and slows down slip processes, thus enhancing strength and resistance to tensile loading. Their distribution within the metallic matrix weakens the bonding between structural components and causes uneven deformation processes. This effect is confirmed by the increased Ti signal observed in the 15 vol% TiC sample, as shown in Fig. 13c, particularly along crack edges and within fracture features, indicating the presence of TiC agglomerates at probable crack initiation sites. It should be noted that EDS analysis of fracture surfaces is subject to well-known methodological limitations due to their highly rough and irregular topography; therefore, only qualitative, not quantitative, analysis is presented. Nevertheless, the observed Ti enrichment in critical fracture regions provides supporting evidence for TiC agglomeration and associated weakening at the phase interface. At the macroscopic scale, this behavior manifests as a significant reduction in ductility compared with other sample groups, which correlates well with the tensile test results.

4. Conclusions

The presented research shows an effect of microstructural heterogeneity on the strengthening and fracture mechanism in *in-situ* cast TiC/Al composites. The new strengthening mechanism is associated with the SHS reaction of TiC carbide formation resulting in heterogeneous distribution of Ti in Al solute solution. This effect, contributes to Hall-Pech relation due to grain refinemnet in saturated regions, Orowan mechanism by interaction of dislocations with nanoparticles and solution strengthening related to higer Ti contration. This opens new perspectives in the design of other *in-situ* cast composites systems. In this contex, the following detailed conclusions can be drawn:

1. Unreacted Ti during the SHS reaction of formation of TiC carbide occurring in liquid aluminum forms nanocrystalline regions of about 10 nm in size of a supersaturated solid solution of titanium in aluminum. This alters the lattice parameter of this solid solution and further refines the grains within the dendritic matrix. As a result, an additional strengthening effect is achieved for the composite.
2. Strength and plasticity of the tested composites are strongly dependent on the amount of TiC particles added, which is associated with other strengthening mechanisms. Tensile tests showed that the investigated composites can be divided into two groups with respect to the reference aluminum Al1000 series alloy (without TiC). The first group, containing 5–10 vol% of TiC, shows a moderate increase in strength and similar plasticity, while the second group containing 15 vol% TiC, demonstrates a strong increase in strength but a reduction in plasticity.
3. Hardness and resistance to abrasive wear increase almost linearly with the TiC content. This behaviour, in combination with mechanical properties, allows the composite properties to be tailored for a specific application.
4. Analysis of fracture mechanisms by observing the fracture surface after the tensile test showed very good agreement with that obtained in the tensile test. The agglomeration of TiC particles, observed in samples with TiC content greater than 10 vol%, was the primary reason for reduced plasticity. This was due to weakened bonding between the particles and the matrix, leading to uneven deformation during loading.

CRediT authorship contribution statement

Wojciech Maziarz: Writing – original draft, Supervision, Project administration, Investigation, Formal analysis, Conceptualization. **Robert Chulist:** Writing – review & editing, Investigation, Formal analysis, Conceptualization. **Ganna Chyzhyk:** Writing – review & editing, Investigation, Formal analysis. **Anna Wojcik:** Writing – review & editing, Investigation, Conceptualization. **Pawel Kurtyka:** Writing – review & editing, Methodology, Conceptualization. **Sebastian Sobula:** Writing – review & editing, Methodology, Conceptualization. **Norbert Schell:** Data curation. **Ewa Olejnik:** Writing – review & editing, Investigation, Conceptualization.

Declaration of competing interest

The authors declare that they have no known competing financial interests or personal relationships that could have appeared to influence the work reported in this paper.

Acknowledgement

Financial support of the National Science Centre, Poland (project no. 2021/43/B/ST8/03271) is greatly acknowledged.

Data availability

Data will be made available on request.

References

[1] J.A. Garcia-Hinojosa, C. González R., J.A. Juárez I, M.K. Surrapa, Effect of grain refinement treatment on the microstructure of cast Al–7Si–SiCp composites, Materials Science and Engineering A 386 (2004) 54–60, https://doi.org/10.1016/j.msea.2004.07.020.
[2] A. Mazahery, H. Abdizadeh, H.R. Baharvandi, Development of high-performance A356/nano-Al_2O_3 composites, Mater. Sci. Eng. A 518 (2009) 61–64, https://doi.org/10.1016/j.msea.2009.04.014.
[3] T. Wang, Y. Zheng, Z. Chen, Y. Zhao, H. Kang, Effects of Sr on the microstructure and mechanical properties of in situ TiB2 reinforced A356 composite, Mater. Des. 64 (2014) 185–193, https://doi.org/10.1016/j.matdes.2014.07.040.
[4] R. Geng, F. Qiu, Q.-L. Zhao, Y.-Y. Gao, Q.-C. Jiang, Effects of nanosized TiCp on the microstructure evolution and tensile properties of an Al-Mg-Si alloy during cold rolling, Mater. Sci. Eng. A 743 (2019) 98–105, https://doi.org/10.1016/j.msea.2018.11.078.
[5] T. Xu, G. Li, M. Xie, M. Liu, D. Zhang, Y. Zhao, G. Chen, X. Kai, Microstructure and mechanical properties of in-situ nano γ-Al_2O_3p/A356 aluminum matrix composite, J. Alloys Compd. 787 (2019) 72–85, https://doi.org/10.1016/j.jallcom.2019.02.045.

[6] W. Qian, X. Kai, X. Liang, R. Cao, G. Chen, Y. Zhao, Insight into microstructure evolution of in-situ ZrB_2np/AA6111 composites with both excellent room and high temperature properties, Mater. Sci. Eng. A 914 (2024) 147161, https://doi.org/10.1016/j.msea.2024.147161.

[7] P. Hariharasakthisudhan, B. Surya Rajan, K. Sathickbasha, Inspiration of reinforcements, manufacturing methods, and microstructural changes on wear behavior of metal matrix composites—a recent review, Mater. Res. Express 7 (2020) 012006, DOI 10.1088/2053-1591/ab6918.

[8] S.L. Pramod, S.R. Bakshi, B.S. Murty, Aluminum-based cast In Situ Composites: a Review, J. Mater. Eng. Perform. 24 (2015) 2185–2207, https://doi.org/10.1007/s11665-015-1424-2.

[9] C. Cao, A. Killips, X. Li, Advances in the Science and Engineering of Metal Matrix, Nanocomposites: a Review, Adv. Eng. Mater. 26 (2024) 2400217, https://doi.org/10.1002/adem.202400217.

[10] Y. Liu, Q. Han, Interaction between nucleant particles and a solid-liquid interface in Al-4.5Cu alloy, 116956, Acta Mater. 213 (2021), https://doi.org/10.1016/j.actamat.2021.116956.

[11] Z. Zhang, D.L. Chen, Contribution of Orowan strengthening effect in particulate-reinforced metal matrix nanocomposites, Mater. Sci. Eng. A 483–484 (2008) 148–152, https://doi.org/10.1016/j.msea.2006.10.184.

[12] D.M. Stefanescu, F.R. Juretzko, A. Catalina, B.K. Dhindaw, S. Sen, P.A. Curreri, Particle engulfment and pushing by solidifying interfaces. II. Microgravity experiments and theoretical analysis, Metall. Mater. Trans. A 29 (1998) 1697–1706, https://doi.org/10.1007/s11661-998-0092-3.

[13] A.V. Catalina, S. Mukherjee, D.M. Stefanescu, A dynamic model for the interaction between a solid particle and an advancing solid/liquid interface, Metall. Mater. Trans. A 31 (2000) 559–568, https://doi.org/10.1007/s11661-000-0200-5.

[14] W. Maziarz, A. Wójcik, R. Chulist, A. Bigos, P. Kurtyka, Ł. Szymański, A. Jimenez-Zabaleta, M. García de Cortázar, E. Olejnik, Microstructure and mechanical properties of Al/TiC and Al/(Ti,W)C nanocomposites fabricated via in situ casting method, J. Mater. Res. Technol. 28 (2024) 1852–1863, https://doi.org/10.1016/j.jmrt.2023.12.126.

[15] J.Q. Xu, L.Y. Chen, H. Choi, X.C. Li, Theoretical study and pathways for nanoparticle capture during solidification of metal melt, J. Phys. Condens. Matter 24 (2012) 255304, https://doi.org/10.1088/0953-8984/24/25/255304.

[16] H.C. Hamaker, The London—van der Waals attraction between spherical particles,.

[17] Physica 4 (1937) 1058–1072, https://doi.org/10.1016/S0031-8914(37)80203-7.

[18] A. Wójcik, E. Olejnik, A. Bigos, R. Chulist, P. Bobrowski, P. Kurtyka, A. Tarasek, N. Rylko, L. Szymanski, W. Maziarz, Microstructural characterization and mechanical properties of in situ cast nanocomposites Al/TiC type, J. Mater. Res. Technol. 9 (2020) 12707–12715, https://doi.org/10.1016/j.jmrt.2020.09.012.

[19] O. El-Kady, A. Fathy, Effect of SiC particle size on the physical and mechanical properties of extruded Al matrix nanocomposites, Mater. Des. 54 (2014) 348–353, https://doi.org/10.1016/j.matdes.2013.08.049.

[20] S. Bathula, R.C. Anandani, A. Dhar, A.K. Srivastava, Microstructural features and mechanical properties of Al 5083/SiCp metal matrix nanocomposites produced by high energy ball milling and spark plasma sintering, Mater. Sci. Eng. A 30 (2012) 97–102, https://doi.org/10.1016/j.msea.2012.02.095.

[21] M. Penchal Reddy, F. Ubaid, R.A. Shakoor, P. Gururaj, M. Vyasaraj, A.M. A. Mohamed, M. Gupta, Effect of reinforcement concentration on the properties of hot extruded Al–Al2 O3 composites synthesized through microwave sintering process, Mater. Sci. Eng. A 696 (2017) 60–69, https://doi.org/10.1016/j.msea.2017.04.064.

[22] L. Jiang, Z. Li, G. Fan, D. Zhang, A flake powder metallurgy approach to Al2 O3 /Al biomimetic nanolaminated composites with enhanced ductility, Scripta Mater. 65 (2011) 412–415, https://doi.org/10.1016/j.scriptamat.2011.05.022.

[23] J. Ni, J. Li, W. Luo, Q. Han, Y. Yin, Z. Jia, B. Huang, C. Hu, Z. Xu, Microstructure and properties of in-situ TiC reinforced copper nanocomposites fabricated via long-term ball milling and hot pressing, J. Alloys Compd. 755 (2018) 24–28, https://doi.org/10.1016/j.jallcom.2018.04.327.

[24] Y. Li, Y.J. Lin, Y.H. Xiong, J.M. Schoenunga, E.J. Lavernia, Extended twinning phenomena in Al–4% Mg alloys/B4 C nanocomposite, Scripta Mater. 64 (2011) 133–136, https://doi.org/10.1016/j.scriptamat.2010.09.027.

[25] Z.H. Zhang, T. Topping, Y. Li, R. Vogt;, Y.Z. Zhou, C. Haines, J. Paras, D. Kapoor, J. M. Schoenung, E.J. Lavernia, Mechanical behavior of ultrafine-grained Al composites reinforced with B4 C nanoparticles, Scripta Mater. 65 (2011) 652–655, https://doi.org/10.1016/J.SCRIPTAMAT.2011.06.037.

[26] L. Jiang, H. Yang, J.K. Yee, X. Mo, T. Topping, E.J. Lavernia, J.M. Schoenung, Toughening of aluminum matrix nanocomposites via spatial arrays of boron carbide spherical nanoparticles, Acta Mater. 103 (2016) 128–140, https://doi.org/10.1016/j.actamat.2015.09.057.

[27] J. Ye, B.Q. Han, Z. Lee, B. Ahn, S.R. Nutt, J.M. Schoenung, A tri-modal aluminum based composite with super-high strength, Scripta Mater. 53 (2005) 481–486, https://doi.org/10.1016/j.scriptamat.2005.05.004.

[28] H. Wu, G.H. Fan, M. Huang, L. Geng, X.P. Cui, H.L. Xie, Deformation behavior of brittle/ductile multilayered composites under interface constraint effect, Int. J. Plast 89 (2017) 96–109, https://doi.org/10.1016/j.ijplas.2016.11.005.

[29] G. Liu, G.J. Zhang, F. Jiang, X.D. Ding, Y.J. Sun, J. Sun, E. Ma, Nanostructured high-strength molybdenum alloys with unprecedented tensile ductility, Nat. Mater. 12 (2013) 250–344, https://doi.org/10.1038/nmat3544.

[30] L.J. Huang, L. Geng, H.X. Peng, Microstructurally inhomogeneous composites: is a homogeneous reinforcement distribution optimal? Prog. Mater Sci. 71 (2015) 93–168, https://doi.org/10.1016/j.pmatsci.2015.01.002.

[31] M. Huang, C. Xu, G. Fan, E. Maawad, W. Gan, L. Geng, F. Lin, G. Tang, H. Wu, Y. Du, D. Li, K. Miao, T. Zhang, X. Yang, Y. Xia, G. Cao, H. Kang, T. Wang, T. Xiao, H. Xie, Role of layered structure in ductility improvement of layered Ti–Al metal composite, Acta Mater. 153 (2018) 235–249, https://doi.org/10.1016/j.actamat.2018.05.005.

[32] Z. Zhang, D.L. Chen, Consideration of Orowan strengthening effect in particulate-reinforced metal matrix nanocomposites: a model for predicting their yield strength, Scr. Mater. 54 (2006) 1321–1326, https://doi.org/10.1016/j.scriptamat.2005.12.017.

[33] L.-Y. Chen, J.-Q. Xu, H. Choi, M. Pozuelo, X. Ma, S. Bhowmick, J.-M. Yang, S. Mathaudhu, X.-C. Li, Processing and properties of magnesium containing a dense uniform dispersion of nanoparticles, Nature 528 (2015) 539–543, https://doi.org/10.1038/nature16445.

[34] D. Hull, D.J. Bacon, Introduction to Dislocations, Butterworth-Heinemann/Elsevier, Amsterdam, 2011.

[35] A. Sanaty-Zadeh, P.K. Rohatgi, Comparison between current models for the strength of particulate-reinforced metal matrix nanocomposites with emphasis on consideration of Hall–Petch effect, Mater. Sci. Eng. A 531 (2012) 112–118, https://doi.org/10.1016/j.msea.2011.10.043.

[36] J.B. Ferguson, I. Aguirre, H. Lopez, B.F. Schultz, K. Cho, P.K. Rohatgi, Tensile properties of reactive stir-mixed and squeeze cast Al/CuOnp-based metal matrix nanocomposites, Mater. Sci. Eng. A 611 (2014) 326–334, https://doi.org/10.1016/j.msea.2014.06.008.

[37] C.-S. Kim, I. Sohn, M. Nezafati, J.B. Ferguson, B.F. Schultz, Z. Bajestani-Gohari, P. K. Rohatgi, K. Cho, Prediction models for the yield strength of particle-reinforced unimodal pure magnesium (Mg) metal matrix nanocomposites (MMNCs), J. Mater. Sci. 48 (2013) 4191–4204, https://doi.org/10.1007/s10853-013-7232-x.

[38] T. Nukami, M.C. Flemings, In situ synthesis of TiC particles-reinforced aluminum matrix composite, Metall. Mater. Trans. A 26 (1995) 1877–1884, https://doi.org/10.1007/BF02670775.

[39] A. Wójcik, R. Chulist, A. Szewczyk, B. Morończyk, Ł. Żrodowski, R. Wróblewski, M. Kowalczyk, A. Kolano-Burian, P. Zackiewicz, N. Schell, W. Maziarz, Microstructure and texture control of Ni-Mn-Ga magnetic shape memory alloys manufactured by laser powder bed fusion, Addit. Manuf. 86 (2024) 104225, https://doi.org/10.1016/j.addma.2024.104225.

[40] R. Chulist, A. Wójcik, A. Sozinov, T. Tokarski, M. Faryna, N. Schell, W. Skrotzki, B. Li, H. Sehitoglu, X. Li, W. Maziarz, Adaptive phase or Variant Formation at the Austenite/Twinned Martensite Interface in Modulated Ni–Mn–Ga Martensite, Adv. Funct. Mater. 34 (2024) 2307322, https://doi.org/10.1002/adfm.202307322.

[41] W. Maziarz, R. Chulist, A. Wójcik, A. Szewczyk, M. Szlezynger, S. Sobula, P. Kurtyka, E. Olejnik, Multiscale microstructure characterisation of Metal Matrix Composites (MMC) reinforced by the ultrafine particles, Arch. Metall. Mater. 70 (2025) 1309–1315, https://doi.org/10.24425/amm.2025.154483.

[42] R. Casati, M. Vedani, Metal Matrix Composites Reinforced by Nano-Particles—A Review, Metals 4 (2014) 65–83, https://doi.org/10.3390/met4010065.

[43] H. Okamoto, Phase diagrams for binary alloys, ASM International, Materials Park, OH, 2000.

[44] S. Hori, H. Tai, E. Matumoto, Solid solubility of titanium in aluminium, J. Jpn. Inst. Light Met. 34 (1984) 377–381.

[45] V.M.J. Sharma, K.S. Kumar, N.B. Rao, S.D. Pathak, Effect of microstructure and strength on the fracture behavior of AA2219 alloy, Mater. Sci. Eng. A 502 (2009) 45–53, https://doi.org/10.1016/j.msea.2008.11.024.

[46] D. Xu, K. Chen, Y. Chen, S. Chen, Evolution of the second-phase particles and their effect on tensile fracture behavior of 2219 Al–xCu alloys, Metals 10 (2020) 197, https://doi.org/10.3390/met10020197.

[47] T.-S. Liu, F. Qiu, S.-L. Shu, S.-Q. Kou, H.-Y. Yang, T.-T. Duan, Q.-C. Jiang, Multilevel microstructure control of cast Al–7.0Si–4.0Cu alloy with high strength–toughness synergy via micro-alloying combined with manipulation by in situ nano ceramics, J. Mater. Res. Technol. 21 (2024) 3248–3261, https://doi.org/10.1016/j.jmrt.2022.10.140.

[48] J. Yang, Y. Zhao, X. Kai, Y. Zhang, Y. Shan, H. Zhu, Synergistic enhancement of in-situ (Al_2O_3 + ZrB_2) nanoparticles and Er on microstructure and stress corrosion resistance of 7075Al matrix composites, J. Mater. Res. Technol. 36 (2025) 6542–6554, https://doi.org/10.1016/j.jmrt.2025.04.287.